JOURNAL OF MAGNETIC RESONANCE 64, 177–182 (1985)

Exploiting the Stimulated Echo in Nuclear Magnetic Resonance Imaging. I. Method

WILLIAM SATTIN,*,†,‡ THOMAS H. MARECI,*,§ AND KATHERINE N. SCOTT*,†,§,‖

*Departments of *Radiology, †Nuclear Engineering Sciences and §Physics, University of Florida, and ‖VA Medical Center, Gainesville, Florida 32610*

Received May 3, 1985

There is an adage that applies equally to all multipulse NMR experiments which states it is easier to induce spin echos than not. Rather than ignore or suppress these additional echos in NMR imaging experiments (*1*) we wish to communicate techniques which glean added information from them. In particular we exploit the unique properties of the stimulated echo as first identified by Hahn (*2*) and further quantified by Woessner (*3*). Although new to NMR imaging, stimulated echos have been successfully applied by Tanner to the measurement of translational self-diffusion coefficients (*4*), by Lausch and Spiess to study infrequent jumps of complex molecules (*5, 6*), and more recently to analyze slow rotational motions of molecular solids by Sullivan *et al.* (*7*). This communication will outline the methodology involved in the execution of stimulated echo NMR imaging. A subsequent communication (*8*) will present specific applications, and is henceforth referred to as Part II.

Consider a spin system in thermal equilibrium with its surroundings subjected to the rf pulse and magnetic field gradient pulse experiment depicted in Fig. 1. We bring the net magnetization into the transverse plane with the transmission (Tx) of a $\pi/2$ rf pulse. Unless stated to the contrary, the rf pulse is of frequency ω_p and width t_p, such that t_p is small compared to T_1 and T_2, and excites the entire chemical shift frequency bandwidth equally. If, for example, the pulse has phase A equal to 0° (i.e., along the positive y direction), the transverse magnetization will initially be aligned with the positive x direction in the rotating frame. Free precession of all isochromats occurs during the time interval τ_1. During this time span we apply pulsed magnetic field gradients as in the conventional Fourier imaging technique (9). The preparatory readout gradient is embodied in the effective x gradient (G_x), whereas G_y and G_z are employed for phase encoding. Obviously z-direction discrimination could also be achieved with a selective $\pi/2$ rf pulse applied in the presence of G_z (*10*).

A second $\pi/2$ rf pulse is applied at the end of the τ_1 interval. Thus far the rf pulse sequence described is simply Hahn's original spin echo experiment (*2*). Hence

‡ To whom correspondence should be addressed c/o Department of Radiology, Box J-374, JHMHC, University of Florida, Gainesville, Fla. 32610.

0022-2364/85 $3.00

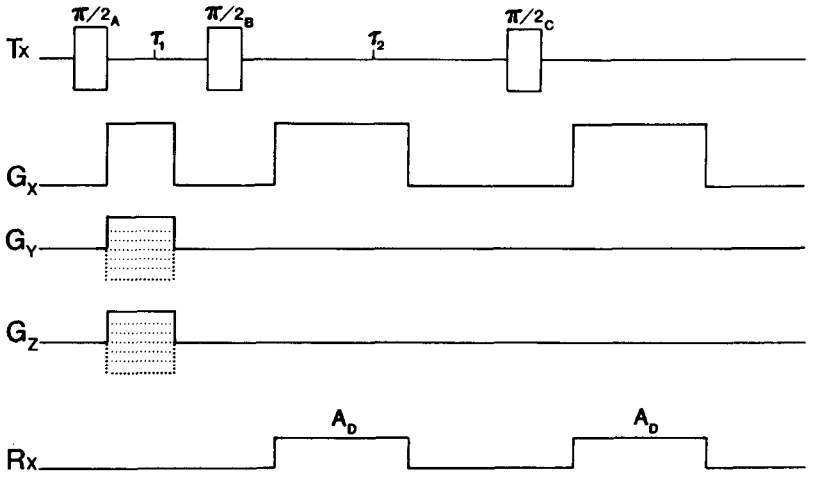

FIG. 1. The stimulated echo imaging pulse sequence. All symbols are defined in the text.

a primary echo is created whose maximum appears at a time τ_1 after the second $\pi/2$ rf pulse, and whose amplitude at this time, M_{PE}, is given by

$$M_{PE} = M_0 \sin\theta_1 \sin^2(\theta_2/2) \exp(-2\tau_1/T_2) f(G, D, \tau_1) \quad [1]$$

where M_0 is the equilibrium magnetization, θ_i represents the $\omega_p t_p$ product for the ith pulse, T_2 is the spin–spin relaxation time, and $f(G, D, \tau_1)$ corresponds to the diffusional damping resulting from the presence of magnetic field gradients. For a constant steady gradient, $f(G, D, \tau_1) = \exp(-\frac{2}{3}\gamma^2 G^2 D \tau_1^3)$, where G is the magnetic field gradient and D the translational self-diffusion coefficient. It should be noted that pulsed magnetic field gradients have been used in this work, hence the functional form of $f(G, D, \tau_1)$ will be different (*11*). The two cases are identical, in the limit, as we pass from pulsed to continuous application of the gradient. Imposing the G_x readout gradient while the primary echo is being received (Rx) will frequency encode the primary echo with x-direction spatial dependence.

For ideal $\pi/2$ rf pulses this primary echo image is identical to the one produced by the conventional $\pi/2$–τ–π spin echo imaging sequence, except for a factor of one-half in signal intensity. This reduction in signal-to-noise would be intolerable unless we can recover it or reap additional benefit. Fortunately the other half of the magnetization is not dissipated, rather it has been stored as longitudinal magnetization by the second $\pi/2$ rf pulse.

It can be shown that the solution to the Bloch equation in the rotating frame (*12*) takes on the form

$$M_x(t + t_p) = M_x(t) \quad [2]$$

$$M_y(t + t_p) = M_y(t)\cos\theta - M_z(t)\sin\theta \quad [3]$$

$$M_z(t + t_p) = M_y(t)\sin\theta + M_z(t)\cos\theta \quad [4]$$

in response to a rf pulse along the x axis commencing at time t such that $\theta = \omega_p t_p$. In this representation the rotating portion of the net magnetization is decomposed

into two orthogonal components. M_x is taken to be in phase with respect to the x-axis rotating frame of reference, while M_y is out of phase. Of prime interest is Eq. [4], which characterizes the longitudinal magnetization, and in particular its dependence on $M_y(t)$. Since the spin system is initially in thermal equilibrium, $M_y(0) = 0$. Hence, by Eq. [4], $M_z(t_p) = 0$ for an ideal $\pi/2$ rf pulse. During the interval τ_1, M_z simply approaches equilibrium magnetization.

If τ_1 is on the order of T_2 or less, then $M_y(\tau_1)$ is surely nonzero. That is, at time τ_1 we will have appreciable transverse magnetization. Therefore the second $\pi/2$ rf pulse, in addition to inducing a primary echo, will also produce net longitudinal magnetization (i.e., $M_z(\tau_1 + t_p) \neq 0$), which retains its phase memory. For the duration of τ_2 the longitudinal magnetization is affected solely by spin–lattice relaxation. Indeed, even the readout gradient for the primary echo does not influence the longitudinal magnetization.

The third $\pi/2$ rf pulse which comes at the end of the τ_2 interval simply rotates the stored longitudinal magnetization back to the transverse plane with a phase reversal, relative to its phase prior to the second $\pi/2$ rf pulse. Since the only phase dispersion this magnetization experienced occurred while it was transverse during the interval τ_1, only a time τ_1 is required for phase refocusing. Hence if $\tau_2 > \tau_1$ the stimulated echo's maximum will appear at a time τ_1 after the third $\pi/2$ rf pulse. The amplitude of the echo at this time, M_{STE}, is given by

$$M_{STE} = \tfrac{1}{2}M_0 \sin\theta_1 \sin\theta_2 \sin\theta_3 \exp[-(2\tau_1/T_2 + \tau_2/T_1)] f(G, D, \tau_1, \tau_2) \qquad [5]$$

where all terms have been previously defined, and $f(G, D, \tau_1, \tau_2)$ is the diffusional damping term for the stimulated echo. For a constant steady gradient, $f(G, D, \tau_1, \tau_2) = \exp[-\gamma^2 G^2 D(\frac{2}{3}\tau_1^3 + \tau_1^2\tau_2)]$, and is modified for pulsed magnetic field gradients (*4*). The relaxation damping term tells the history of the magnetization that went into this echo's formation. Since spin–lattice relaxation occurred only within the interval τ_2, magnetization must have been stored in the longitudinal direction during that interval. Likewise, the magnetization can be traced to the transverse direction in the τ_1 interval and also for a time τ_1 subsequent to the third rf pulse, hence the T_2 dependence. Imposing a G_x readout gradient while the Rx window A is gated open will frequency encode the stimulated echo with x-direction spatial dependence. For ideal $\pi/2$ rf pulses, and ignoring relaxation and diffusion damping, we see from Eq. [5] that M_{STE} is proportional to $\frac{1}{2}M_0$. This is the other factor of one-half we noted earlier after the formation of the primary echo. Whereas the conventional $\pi/2$–τ–π spin echo imaging experiment yields a single image whose intensity is proportional to M_0, the $\pi/2$–τ_1–$\pi/2$–τ_2–$\pi/2$ imaging experiment yields two images, each of which is proportional to $\frac{1}{2}M_0$. The utility of these images lies not in this proportionality, but rather in the unique T_1 dependence of the stimulated echo image. Applications which exploit this T_1 dependence will be presented in Part II.

A drawback to the stimulated echo imaging sequence as described is its insensitivity to signed phase information. Because there is only pure amplitude modulation of the signal as a function of the interval τ_1, it would normally be necessary to set the Tx frequency outside the spectrum, employ single-phase detection, and use only one-sided phase encoding gradients to avoid aliasing. Fortunately a simple modification afforded by phase cycling will circumvent this problem by converting the

amplitude modulation into phase modulation. The two-step phase cycling, used in conjunction with quadrature detection, consists of the first two acquisitions as depicted in Table 1. Here A, B, C, D refer to the phases of the $\pi/2$ rf pulses and Rx as denoted in Fig. 1. Nagayamo *et al.* have used a closely related phase cycling procedure in spin-echo correlated spectroscopy (*13*). Although the two-step sequence is adequate, it behooves us to extend the sequence to four steps to suppress artifacts resulting from longitudinal magnetization recovery during the interval τ_1 (*14*). The four-step phase cycling is illustrated in its entirety in Table 1. The phases of B and C are arbitrary, as long as they remain equal and constant throughout the entire experiment. In practice, an additional spoiling pulsed magnetic field gradient was applied immediately following the primary echo's readout gradient and prior to the third $\pi/2$ rf pulse, along G_x. This reduces artifacts in the stimulated echo image by eliminating the three other possible overlapping secondary echoes which may occur after the third rf pulse. Since the stimulated echo's magnetization is stored along the longitudinal direction during τ_2, the spoil pulse disperses only the transverse magnetization which would have gone on to create additional secondary echoes subsequent to the third rf pulse.

Figure 2 presents typical results from a ^{1}H stimulated echo imaging sequence. The experiments were conducted on a Nicolet (GE-NMR) NT-80 spectrometer with an Oxford 80/310 HR superconducting magnet operated at 1.89 T, with a clear bore diameter of 31 cm. The Oxford 2320 room temperature shim power supply was modified to improve response time and was controlled via the Nicolet 293C pulse programmer through a gating circuit. Controlling software was written in Nicolet 1280 assembly language. The 20 bit deep data were scaled to 5 bits and transferred to a Cromemco Z-2D computer for processing and display.

The phantom shown in Fig. 2a is a red Delicious apple with a 1 cm diameter vial of $CuSO_4$ doped distilled water embedded in its center, dubbed the "William Tell phantom." Figure 2b is the primary echo image and Fig. 2c the stimulated echo image. No G_z phase encoding was performed, resulting in z-direction averaged images (into the page). The G_x readout gradient was 0.5 mT/m, and was applied for 32 ms. There were 64 equal steps of the G_y phase encoding gradient, ranging from 0.5 to -0.5 mT/m, each applied for 16 ms. The data matrix of each image consisted of 128 $\times$ 64 complex data points. The field of view was 10 $\times$ 10 cm, corresponding to a resolution of 1.5 (horizontal) $\times$ 0.75 mm (vertical). Four signal averages were done to take advantage of the four-step phase cycling. Thus all data

TABLE 1

Four-Step Phase Cycling Used in Stimulated Echo Imaging

Acquistion	A	B	C	D
1	0°	0°	0°	0°
2	270°	0°	0°	90°
3	180°	0°	0°	180°
4	90°	0°	0°	270°

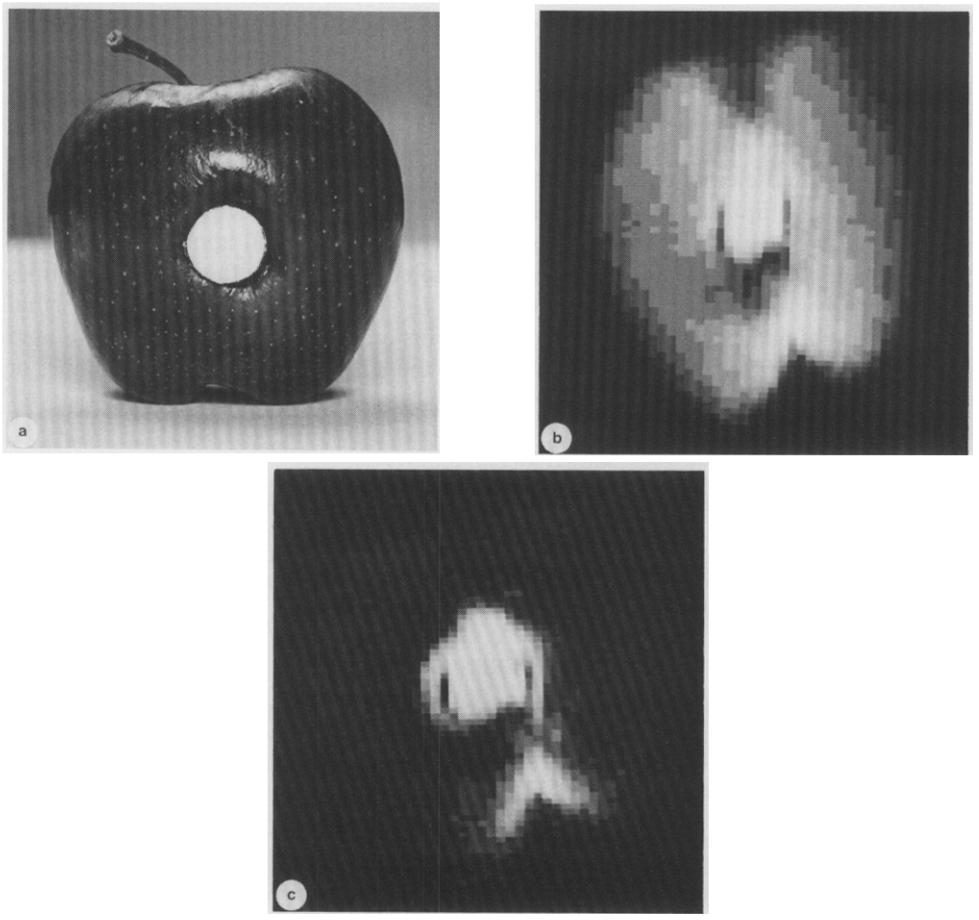

FIG. 2. The "William Tell phantom" (a) *au naturel,* (b) as it appears when the primary echo is used for image construction (τ_1 = 20 ms), (c) as it appears when the stimulated echo is used for image construction (τ_1 = 20 ms, τ_2 = 586 ms).

for both images were collected in 9.4 min. The $\pi/2$ pulse width was 260 μs, repetition of the entire sequence occurred every 2.2 s, with $\tau_1 = 20$ ms and $\tau_2 = 586$ ms.

Owing to a short τ_1, the doped water and apple flesh do not vary greatly in intensity in the primary echo image. Most of the variation in intensity within the apple is due to volume averaging, except for the region of low intensity directly beneath the water vial. This appears to be the area of low flesh density where the seeds reside. The source of high intensity at the base of the apple is not known with certainty, but could be the result of a bruise.

The T_1 of the doped water solution was determined to be 513 $\pm$ 17 ms by an inversion recovery sequence utilizing a composite π pulse without applied gradients. In a similar fashion the T_1 of apple flesh was determined to be less than 200 ms. This spread is dramatically demonstrated in Fig. 2c by the stimulated echo image.

Exploiting stimulated echoes in NMR imaging actually involves the prudent use of the T_1 dependence on echo damping afforded by the stimulated echo. Possible applications abound. One may calculate quantitative T_1 information from the stimulated echo images. In chemical shift imaging different T_1 weighting of the various chemically shifted species could result in images with enhanced or suppressed chemically shifted elements. The addition of a fourth rf pulse to the sequence opens the door to multipulse imaging with intrinsic T_1 weighting. Examples of these applications will appear in Part II. Beyond the direct T_1-related applications lies the possibility of characterizing translational diffusion coefficients with stimulated echoes (*4*). Since *in vivo* T_1 is typically greater than T_2, the effect of relaxation on signal intensity might be lessened by observing the diffusional attenuation of the stimulated echo rather than that of the primary echo in the $\pi/2$–τ_1–$\pi/2$–τ_2–$\pi/2$ sequence, or the spin echo in the $\pi/2$–τ–π sequence.

ACKNOWLEDGMENTS

Kudos to J. F. Fitzsimmons and R. G. Thomas for design and construction of the rf transmit/receive coil and the pulsed gradient interface, M. D. Cockman and J. T. Mao for assembly language software development, L. T. Fitzgerald for image processing and display software, and N. J. Smith for manuscript preparation. This research was supported by grants from the National Institutes of Health (P41-RR-02278) and the Veterans Administration Medical Research Service.

REFERENCES

1. J. H. DUIJN, J. H. N. CREYGHTON, AND J. SMIDT, "Abstracts of Papers," Third Annual Meeting of the Society of Magnetic Resonance in Medicine, New York, New York, August 17–23, 1984.
2. E. L. HAHN, *Phys. Rev.* **80,** 580 (1950).
3. D. E. WOESSNER, *J. Chem. Phys.* **34,** 2057 (1961).
4. J. E. TANNER, *J. Chem. Phys.* **52,** 2523 (1970).
5. M. LAUSCH AND H. W. SPIESS, *Chem. Phys. Lett.* **71,** 182 (1980).
6. H. W. SPIESS, *J. Chem. Phys.* **72,** 6755 (1980).
7. N. S. SULLIVAN, D. ESTÈVE, AND M. DEVORET, *J. Phys. C* **15,** 4895 (1982).
8. W. SATTIN, T. H. MARECI, AND K. N. SCOTT, *J. Magn. Reson.*, in press.
9. W. A. EDELSTEIN, J. M. S. HUTCHISON, G. JOHNSON, AND T. REDPATH, *Phys. Med. Biol.* **25,** 751 (1980).
10. D. I. HOULT, *J. Magn. Reson.* **26,** 165 (1977).
11. E. O. STEJSKAL AND J. E. TANNER, *J. Chem. Phys.* **42,** 288 (1965).
12. F. BLOCH, *Phys. Rev.* **70,** 460 (1946).
13. K. NAGAYAMO, K. WÜTHRICH, AND R. R. ERNST, *Biochem. Biophys. Res. Commun.* **90,** 305 (1979).
14. A. BAX, R. FREEMAN, AND G. MORRIS, *J. Magn. Reson.* **42,** 104 (1981).